Local potential measurement through reference electrodes in vanadium redox flow batteries: evaluation of overpotentials and electrolytes imbalance

M. Cecchetti, A. Casalegno, M. Zago*

Politecnico di Milano, Department of Energy, Via Lambruschini 4, 20156 Milano, Italy

* corresponding author: matteo.zago@polimi.it

Abstract

Vanadium redox flow battery performance is actually hindered by increased overpotentials at high current, due to poor electrochemical activity of the most commonly used carbon electrodes and to electrolyte distribution, implying local mass transport limiting conditions. Moreover, vanadium cross-contamination leads to coulombic efficiency reduction and uncontrolled electrolytes imbalance. This work presents the application of through-plate reference electrodes at inlet and outlet of both positive and negative electrodes. The utility of the electrodes potential measurement is firstly demonstrated in the identification of a relation between electrolytes potential and the corresponding state of charge. Subsequently, local overpotentials and impedance spectra at both electrodes are evaluated, evidencing that the negative electrode is kinetically dominated and presents high overpotential even at low current, while the positive exhibits mass transport effects at high current, especially at cell outlet. Finally, during cycling operation with fixed capacity reference electrode measurements permit to monitor electrolytes imbalance induced by cross-contamination, that mainly affects negative electrolyte. Moreover, additional insights into electrodes potential loss during cycling are provided.

Keywords: cross-contamination, electrolyte imbalance, overpotential, reference electrodes, VRFB.

1. Introduction

Vanadium redox flow battery (VRFB) is a promising technology for energy storage due to its peculiarity to separate power and energy, its high efficiency and extremely long charge/discharge cycle life [1–4]. However, the commercialization of VRFB continues to be hindered by technological issues, among which low specific surface area and poor electrochemical activity of the most commonly used carbon materials [5] and the mass transport of the electrolyte over the porous electrode [4,6], leading to increased overpotential at high current and limited system power density [7,8]. Moreover, even though VRFB employs the same element in different oxidation states in both electrolytes, vanadium cross-over induces side reactions [9] and leads to an undesired variation of electrolyte state of charge (SoC), that occurs with a different intensity at the two half-cell, implying electrolyte imbalance and battery capacity loss [9,10].

The quantification of electrodes overpotential and electrolytes SoC is fundamental for VRFB improvement and components optimization; thus, the development of local and reliable reference electrodes becomes crucial to address these critical issues. Additionally, during system lifetime local potential measurements can reveal which region of the cell is undergoing severe degradation or working in limiting condition, providing useful insights on the adoption of suitable operating strategy and components replacement.

In the literature only limited effort has been dedicated to the development of reference electrode in VRFB; the most of the works [11–14] report the application of dynamic hydrogen electrodes (DHE) in both *sandwich type* or *edge type* configuration. The former is a platinum wire inserted between two membranes, altering cell performance, while the latter is a platinum wire applied on the border of the membrane outside the area defined by the electrode, introducing edge effects in the measurement.

Aaron et al. [11] inserted a DHE between two Nafion® membranes and observed higher potential loss at the negative electrode. In [15] individual electrode impedance were performed and the spectra derived from the negative exhibited high-frequency semi-circular features that were ascribed to a process limited by kinetic. In [12] DHE was used to study half-cell reactions in a vanadium-air battery, highlighting that the cathodic reaction limits system efficiency. In [13] DHE with resistor design was coupled with galvanostatic intermittent titration technique to determine the equilibrium electrode potential for both electrodes, providing a deeper understanding of the observed double-step OCV decay. However, in these works [11–13] no local information about the distribution of electrodes potential and the corresponding impedance spectra were provided.

Mench et al. [16] first developed an experimental method for the measurement of local potential within a multi-layered electrode at the positive side of VRFB. Through-plane potential measurements permitted the evaluation of vanadium concentration and the location of reaction, indicating a mass transfer limited situation with increasing current density.

C. Roth et al. [17] placed in the inlet and outlet tubing of a VRFB two Ag/AgCl reference electrodes, working as Luggin capillaries. The measured voltages between the reference electrodes and the half-cell electrode were used to compare the performance of pristine and thermally oxidized carbon felts at both negative and positive electrodes. In a recent work [18], a similar set-up was adopted to analyze electrode degradation during cycling with different cut-off voltages. However, the Ag/AgCl reference electrode set-up [17,18] does not permit the measurement of actual electrodes potential.

In this work, the system of through-plate reference hydrogen electrodes already proposed by NPL for polymer electrolyte fuel cell is adopted [19] and locally applied in-plane to VRFB. It consists in salt bridges passing through the end plates of the cell, creating an ionic contact between the electrode and a reference hydrogen electrode placed outside the cell. This

configuration permits the local measurement of electrolytic potential [19]. In [14], one single through-plate reference electrode was already applied to evaluate potential loss in a regenerative hydrogen-vanadium fuel cell, but only OCV condition was analysed with electrochemical impedance spectroscopy.

In this work, through-plate reference electrodes are introduced at inlet and outlet of both positive and negative VRFB electrodes, providing an insight into the evaluation of local overpotentials, electrolyte imbalance and electrodes potential loss during system cycling.

2. Experimental

2.1 Experimental setup

The cell active area was 25 cm^2 with single serpentine graphite distributors. The membrane was Nafion® 115 and both positive and negative electrodes were SGL 39 AA carbon paper (nominal thickness of ~290 μm, compressed to 230 μm). The cell temperature was maintained at ambient temperature of 23±2°C. In the hydraulic circuit of each electrolyte a pulse dampener [20,21] was introduced to get rid of flow rate fluctuations induced by the peristaltic pump (Watson-Marlow 323Du with a 314Dw 4 roller headpump). A potentiostat (Material Mates 350-R, current range 10A/-30A, voltage range -12V/+12V) was used to perform polarization curves and cycling, while electrodes impedance spectra were recorded with a potentiostat (Autolab PGSTAT 30®) equipped with a frequency response analyzer module.

The positive and negative electrolyte solutions were prepared according to the procedure reported in [22], starting from a mixture of 1M vanadium IV sulfate oxide hydrate (Alfa Aesar) and 5M sulfuric acid (Fischer Chemicals). The volume of each electrolyte was 300 ml in order to have a sufficient quantity of solution to perform polarization curves assuming a constant SoC. Additionally, the bottles containing the electrolyte were maintained pressurized with N_2 to avoid air infiltration.

2.2 Reference electrodes

The local reference electrode measurement setup, along with the related operating principle, has been extensively described in [19]. In this work it has been applied to VRFB and it consisted in a Nafion® tube salt bridge (diameter 0.64 mm) inside a protective PTFE tubing (diameter 0.84 mm). The salt bridge was saturated with 5M sulfuric acid to guarantee the necessary proton conductivity and to directly connect the surface of VRFB working electrode with a 5M sulfuric acid electrolyte solution, in which a Gaskatel HydroFlex® reversible hydrogen electrode (RHE) was immersed. In order to provide an insight into local VRFB performance and electrolytes imbalance, two measurement points were introduced at both positive and negative electrode, close to the inlet and the outlet of cell active area. A schematic of the experimental set-up is reported in Fig.1.

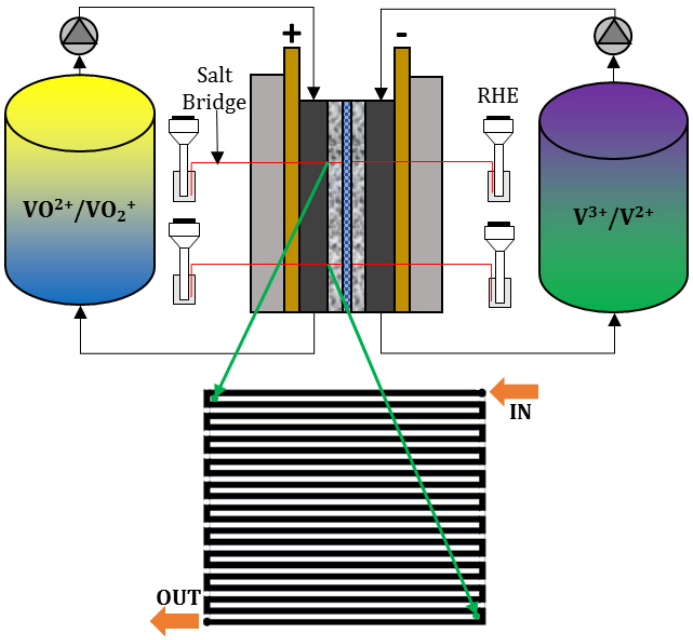

Figure 1 – Schematic of experimental set-up.

2.3 Experimental tests

2.3.1 Relation between potential measurements and SoC

In the literature VRFB models showed discrepancies with experiments in the evaluation of open circuit voltage (OCV) [23], resulting in imprecise relations between OCV and battery SoC [24]. Moreover all the presented models were validated with respect to cell OCV, implying possible inaccuracies in the evaluation of negative and positive electrolytes SoC. In this work, since positive and negative electrode open circuit potential[1] (OCP) were measured, an experimental relation between electrodes OCP and the corresponding electrolyte SoC was adopted. These relations were obtained starting from a fully discharged battery: in this condition the negative and positive electrolytes are respectively composed by vanadium ions V^{3+} and VO^{2+} and the measured electrodes OCP corresponds to SoC 0%. Then the battery was charged in multiple steps at fixed capacity (725 C) and electrodes OCP was monitored until the charging current reached 5 mA at 1.8 V. In this condition the battery is fully charged and the measured electrodes OCP corresponds to SoC 100%. Afterwards it was thus possible to determine the relation between electrode potential and corresponding electrolyte SoC in the whole range of SoC.

2.3.2 Polarization curves and impedance spectra

Polarization curves were performed in galvanostatic mode following one-way curve increasing the current density by steps of 0.05 A cm^{-2}, with each step being held for 45 s, until one among positive and negative electrode potentials reached the limiting value of 0.5 V. In order to investigate a wide range of operating current densities, generally up to 0.55 A cm^{-2}, polarization curves were measured only during discharge, since the charge was limited by hydrogen evolution at the negative electrode [25]. Even though the current density during normal charge-discharge cycles are considerably lower in order to obtain an energetic efficiency around 80%, polarization curves at high current density highlight the limiting phenomena and enhance the

[1] In open circuit, since the reaction overpotentials are null, the measured OCP at positive and negative electrode corresponds to the relative electrolyte potential.

differences between cell inlet and outlet. The investigated operating conditions were SoC 50% at different flow rates: 10, 40 and 100 ml min^{-1}. The positive and negative electrode overpotentials at cell inlet and outlet were calculated as the difference between the electrode OCP[2] and the potentials measured during operation.

Local impedance at the positive (negative) electrode was recorded with a three electrode configuration, applying working and sensing electrode of the potentiostat to the positive (negative) electrode of the cell, the counter electrode to the negative (positive) of the cell and the reference electrode to the external RHE. The impedances spectra were measured in galvanostatic mode only at 0.05 A cm^{-2} in order to limit the SoC variation during the measurement. The amplitude of the sinusoidal signal was 0.01 A cm^{-2} and the frequency range was 10 kHz to 10 mHz with a logarithmic distribution.

2.3.3 Charge-discharge cycles

Two different types of charge-discharge cycles were performed. The first one consisted of 100 cycles at 100 mA cm^{-2} and 40 ml min^{-1}, with 1.1 V and 1.8 V as lower and upper voltage limits [26], respectively. The second one was composed by 20 charge-discharge cycles at 50 mA cm^{-2} and 40 ml min^{-1}, in which charge and discharge time was fixed at 1 hour in order to maintain a coulombic efficiency equal to 1. A lower value of operating current density has been chosen in order to maintain the duration of each charge and discharge step equal to 1 hour without exceeding the safe operating potentials window. In both cycle types, after each charge and discharge step the cell was kept in OCV for 1 minute in order to acquire both cell OCV and electrodes OCP for the evaluation of battery and electrolytes SoC. These quantities are then used to detect and monitor possible electrolytes imbalance.

[2] Considering the electrolyte volume and the time necessary for the measurement of one polarization curve, the reference electrode OCP can be assumed as constant during the measurement.

3. Results and discussion

3.1 Relation between potential measurements and SoC

The relation between positive and negative electrodes OCP[3] (i.e., electrolyte potential) and the corresponding SoC is reported in Fig. 2. The shape of the obtained curves is consistent with Nernst's law [23]: the positive electrode OCP at SoC 100% and 0% are 1.282 V and 0.981 V, respectively; while for the negative electrode, OCPs equal to -0.433 V and -0.174 V correspond to a SoC of 100% and 0%. The definition of these relations is fundamental in order to detect possible electrolytes imbalance. In the literature, the evaluation of positive and negative electrolytes SoC is usually performed regressing the corresponding values from cell OCV exploiting Nernst's law [18]: such an approach would not permit to estimate electrolytes SoC with a reduced uncertainty.

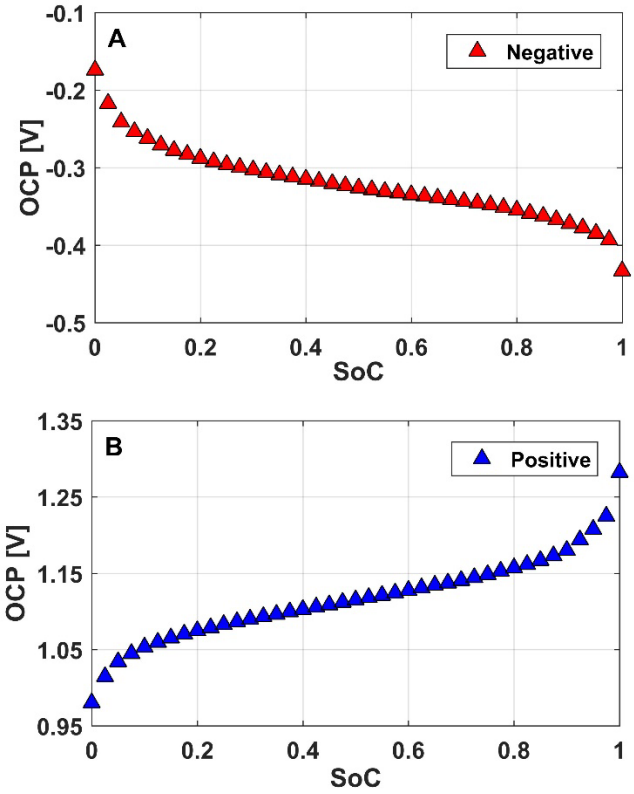

Figure 2 – Experimental relation between electrolyte potential and the corresponding SoC: A) negative electrolyte; B) positive electrolyte.

[3] At open circuit, electrode OCP at inlet and outlet are equal.

Moreover, the difference between the measured cell OCV and the one calculated as the difference between the acquired positive and negative electrode OCP at cell inlet or at cell outlet is always included in 5 mV, confirming the reliability of reference electrodes measurement setup. The resulting value of cell OCV at SoC 50% is equal to 1.457 V, coherently with the values reported in the literature [18,26,27].

3.2 Overpotentials evaluation

Polarization curves have been performed with different flow rates at SoC[4] 50%: Fig. 3 reports the comparison between positive and negative electrode overpotentials at cell inlet and outlet. As expected, higher flow rates imply a reduction of overpotential at both cell inlet and outlet, induced by the increased reactants stoichiometry.

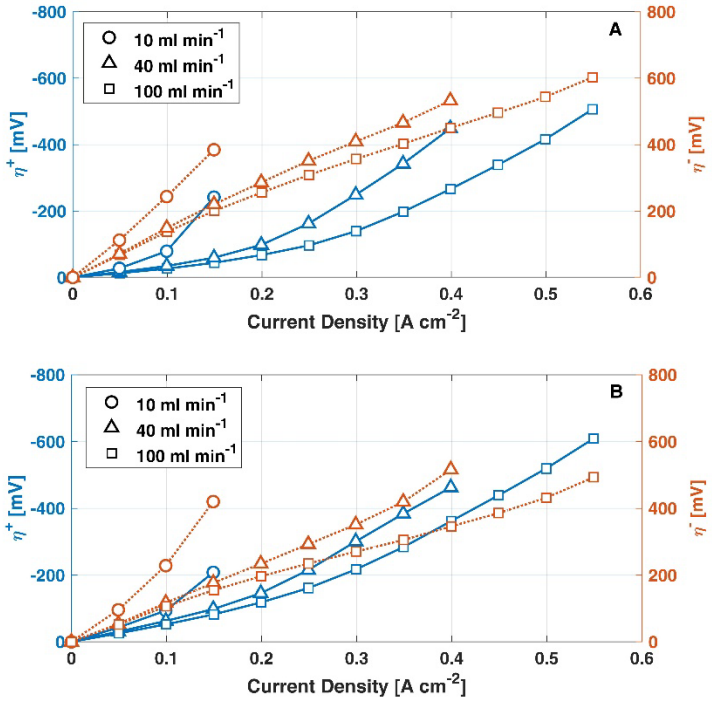

Figure 3 – Positive (solid) and negative (dotted) electrode overpotentials at different flow rates: A) cell inlet; B) cell outlet.

[4] The difference between reference electrodes OCP before and after the measurement of a polarization curve was always lower than 5 mV, corresponding to a variation of SoC inferior to 5%.

Fixing the flow rate and the operating current, at cell inlet (Fig. 3A) negative electrode overpotential is always higher compared to the positive one, indicating that the potential losses at the negative are predominant in the whole range of investigated operating conditions. Moreover, negative electrode overpotentials present a steep linear trend, typical of sluggish kinetic not limited by mass transport phenomena, while the positive ones exhibit an exponential behavior, evidencing the occurrence of mass transport losses at high current densities. These findings are in agreement with the theoretical viscosity values reported in [28], in which the positive electrolyte has higher viscosity than the negative one, resulting in increased mass transport resistance through the porous electrode. This consideration is only valid in the investigated operating conditions, because the electrolytes viscosity has been proved to be strongly variable with operating conditions [29–32], such as temperature and concentrations of vanadium and sulfuric acid.

Considering cell outlet (Fig. 3B), overpotentials behavior does not change substantially: at the negative the reaction is kinetically dominated, while at the positive mass transport losses occur at high current. With serpentine flow field, electrolytes distribution over the porous electrode is more critical at cell outlet [33] and in fact positive overpotentials are higher in this region of the cell, where mass transport losses are enhanced. For current densities greater than 0.4 A cm^{-2}, positive electrode overpotential is even higher compared to the negative one. The latter is minor at cell outlet (Fig. 3B) compared to cell inlet (Fig. 3A). Considering that the cell voltage difference is the same over the active area and assuming a constant ohmic drop through the membrane, this overpotential behavior is physically consistent. At cell outlet increased overpotential at the positive are compensated by overpotential reduction at the negative, that can be due to a lower value of local current density, not measured by the reference electrode.

Local impedance spectra of negative and positive electrode performed at 0.05 A cm^{-2} and 40 ml min^{-1} are reported in Fig. 4A and 4B, respectively. Even at low current, two clear impedance

features are observable: the first one, whose relaxation frequency is included between 10 and 20 Hz, is typical of kinetic phenomena, while the second one, at frequency lower than 1 Hz, is generally addressed to mass transport losses [21]. At the positive electrode, the impedance feature ascribed to electrode kinetic is considerably smaller compared to the one related to mass transport, while at the negative, the contribution of kinetic losses to EIS total resistance becomes relevant. Comparing negative (Fig. 4A) and positive (Fig. 4B) electrode impedance spectra, it is evident that the negative ones exhibit worse kinetic and higher total resistance, further supporting the overpotential measurements reported in Fig. 3.

The difference between EIS at cell inlet and outlet is minor and this is coherent with the limited operating current; but for a more rigorous comparison, the local value of current density is fundamental.

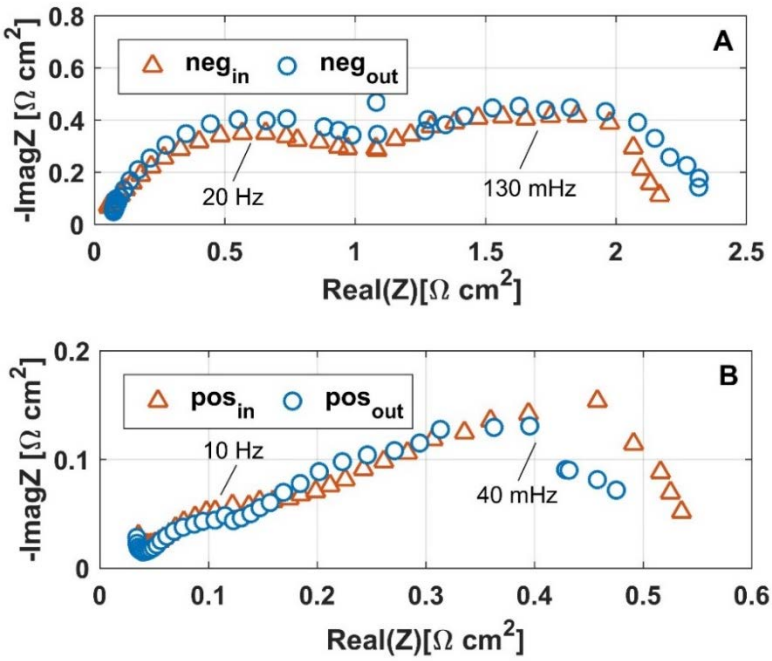

Figure 4 – Local EIS at 0.05 A cm^{-2} and 40 ml min^{-1}: A) negative electrode; B) positive electrode.

3.3 Cycling analysis

Figure 5A reports cell voltage during charge-discharge cycles at 100 mA cm^{-2}: an evident capacity reduction and decrease in battery energetic efficiency are observable. These results are coherent with the cycling operation reported in [18], where after 50 cycles at 0.1 A cm^{-2} with fixed cut-off voltages a comparable cell voltage trend was obtained. Analyzing evolution of negative electrode potentials (Fig. 5B), it is noticeable a severe potential loss during discharge at the negative, while during charge the potential loss keeps nearly constant. At the positive (Fig. 5.C), electrode potential loss with cycling is similar in both charge and discharge. According to [18,34], the observed potential losses are caused by a coupled effect of electrodes degradation and electrolyte imbalance induced by cross-contamination.

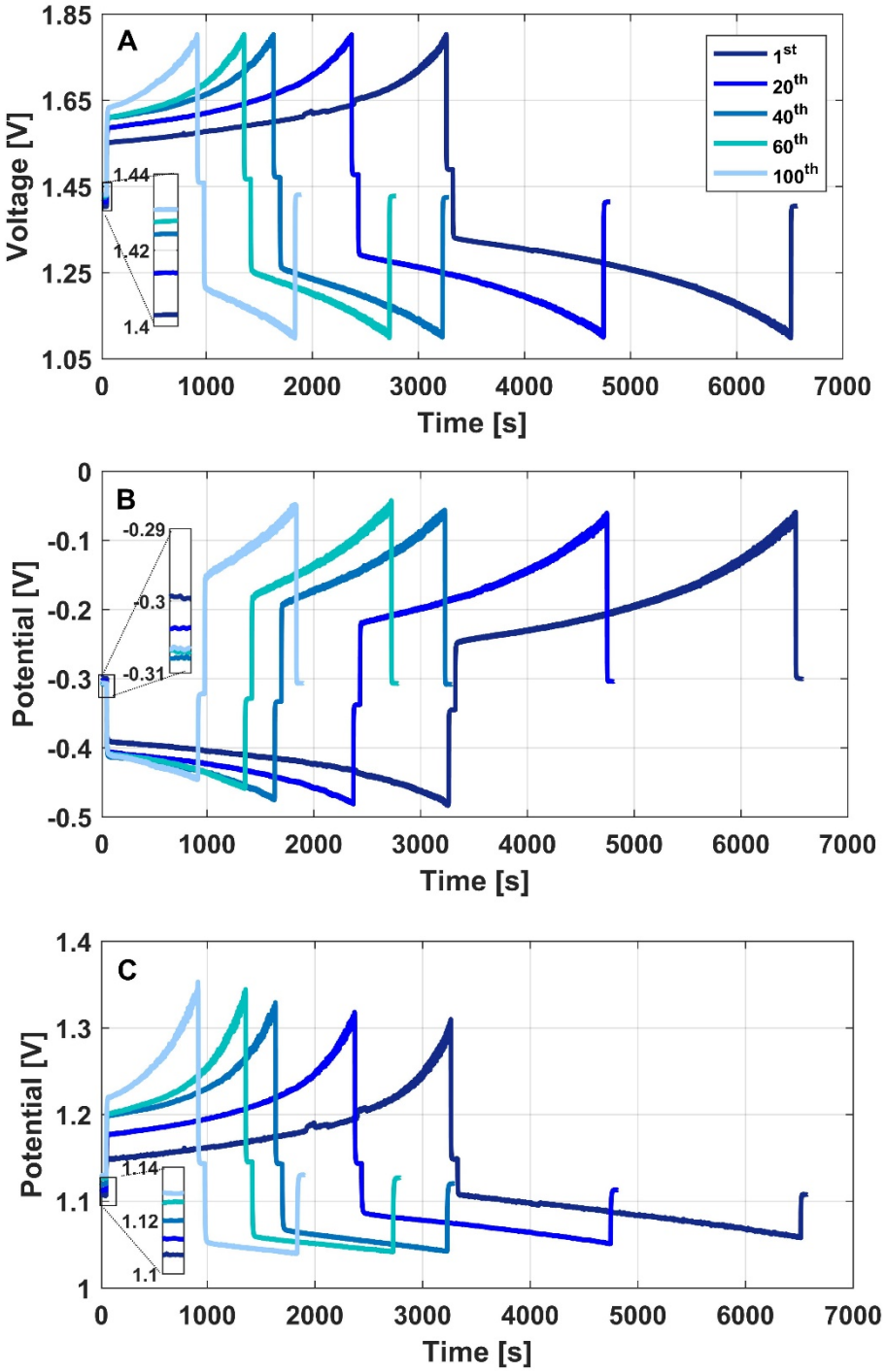

Figure 5 – Charge-discharge cycles at 100 mA cm^{-2}: A) cell voltage; B) negative electrode potential; C) positive electrode potential.

The evolution of electrodes potential at cell outlet is not reported for the sake of brevity, since the behavior is similar to the one reported for cell inlet (Fig. 5B and 5C). In the investigated operating condition (100 mA cm^{-2} and 40 ml min^{-1}), since the electrolytes SoC is always

included between 20 and 80%, no severe reactants starvation occurs and the differences between electrode potentials at cell inlet and outlet are minor, in agreement with the overpotentials at SoC 50% of Fig. 3.

Electrode degradation, along with cross-contamination, leads to battery capacity reduction, resulting in a variation of OCV at the end of each charge and discharge. In particular, cell OCV tends to decrease before each discharge (inset in Fig. 5A) and the opposite occurs before each charge. This is clearly illustrated in Fig. 6A, in which the variation of battery OCV during cycling is nearly symmetric: between the first (cycle 1) and last (cycle 100) charge the battery SoC reduces by roughly 15%, while in discharge it shows a similar increase. This suggests that the combined effect of degradation and cross-contamination has got a comparable influence on the variation of battery SoC.

However, as previously explained, cell OCV is not reliable in the evaluation of possible electrolytes imbalance induced by cross-contamination. For this reason electrodes OCP at the end of each charge and discharge was monitored during cycling to provide an estimate of the two half-cell electrolytes SoC (Fig. 6B and 6C).

Considering the positive electrode (Fig. 6C), the OCP at the end of the charge reaches a stable value after 20 cycles, while the one before the discharge continuously increases until cycle 80 and then it stabilizes, evidencing that during cycling positive electrolyte is discharged towards higher SoC values. Considering the negative electrolyte (Fig. 6B), the behavior is the opposite: electrode OCP is stable after the discharge and it increases at the end of each charge, indicating that the negative electrolyte is continuously charged to lower SoC.

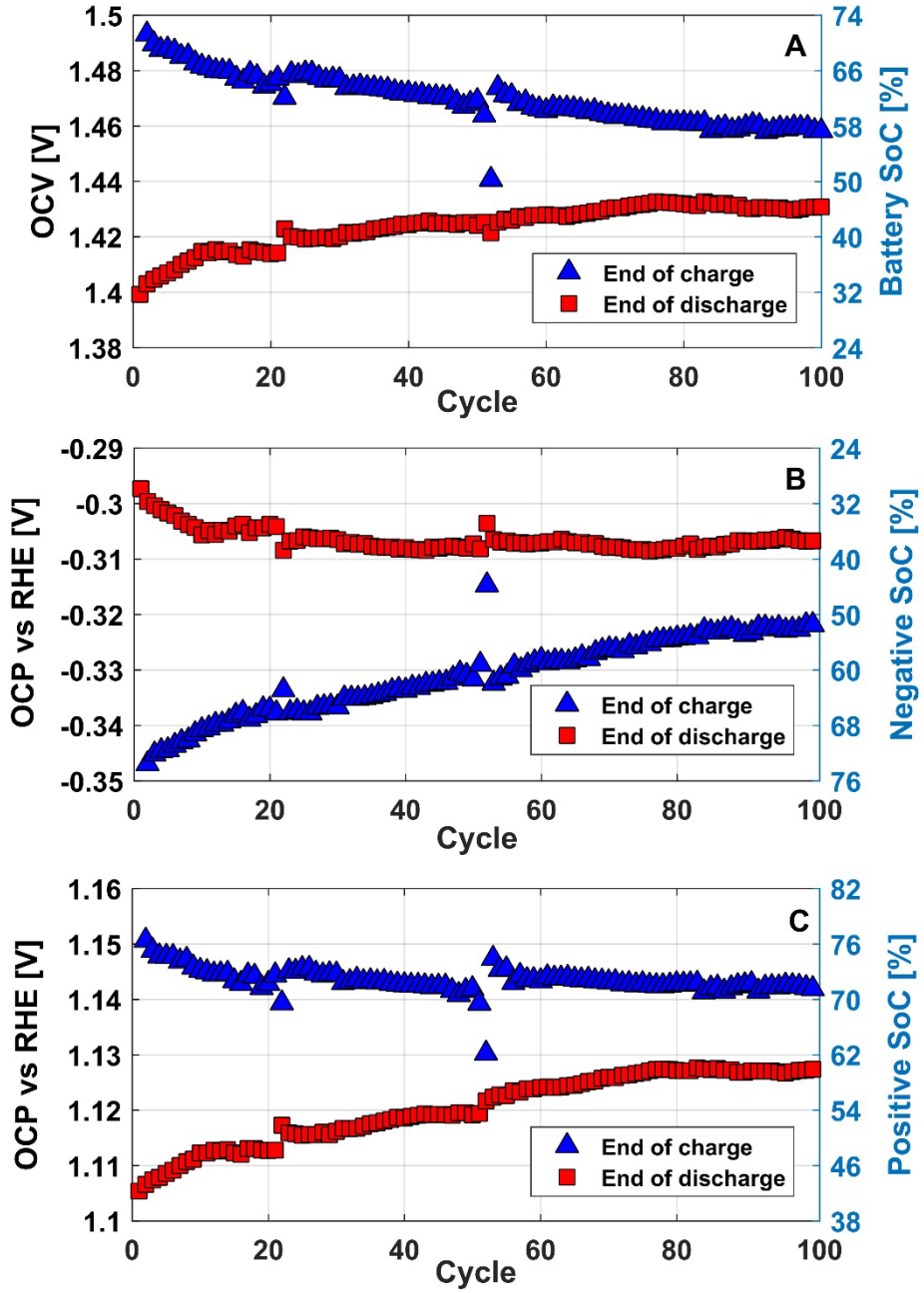

Figure 6 – Evolution during 100 charge-discharge cycles at 100 mA cm^{-2} of A) cell OCV and battery SoC; B) negative electrode OCP and SoC; C) positive electrode OCP and SoC.

These results are coherent with the evolution of electrodes potentials during cycling (Fig. 5B and 5C): at the negative mass transport effects appear towards the end of each discharge cycle, while at the positive mass transport losses affect the final part of charge cycles.

At cycle 1 positive and negative electrolytes are almost balanced: the positive electrolyte SoC varies in the range of 40-75%, while the negative in the range of 30-75%. Instead, at cycle 100

positive electrolyte is included between SoC 60 and 72%, while the negative one between SoC 38 and 50%. As previously stated, this trend of SoC is due to a combined effect of cross-contamination and electrode degradation: the former leads to capacity reduction and electrolyte imbalance, while the latter mainly lowers battery capacity and energetic efficiency. In order to decouple the effect of capacity reduction and clearly evaluate the imbalance due to cross-contamination, 20 cycles at 50 mA cm^{-2} imposing the same time (i.e., capacity) during charge and discharge have been performed. By fixing the capacity during each charge and discharge, a variation of battery and electrolytes SoC can be only caused by vanadium cross-contamination[5]. The measured cell OCV and electrodes OCP at the end of each charge and discharge are reported in Fig. 7. It is noteworthy that during cycles at fixed capacity the battery is continuously undergoing discharge in time (Fig. 7A), indicating that cross-contamination results in battery self-discharge. At the negative electrode (Fig. 7B), a strong SoC reduction is observable, while at the positive (Fig. 7C) the electrolyte SoC shows only a minor decrease, evidencing that the effect of cross-contamination is still present but less intense compared to the negative half-cell.

[5] The presence of hydrogen evolution is avoided preventing the negative electrode to exceed -420 mV vs. RHE, while its onset potential has been measured to be lower than -500 mV vs. RHE.

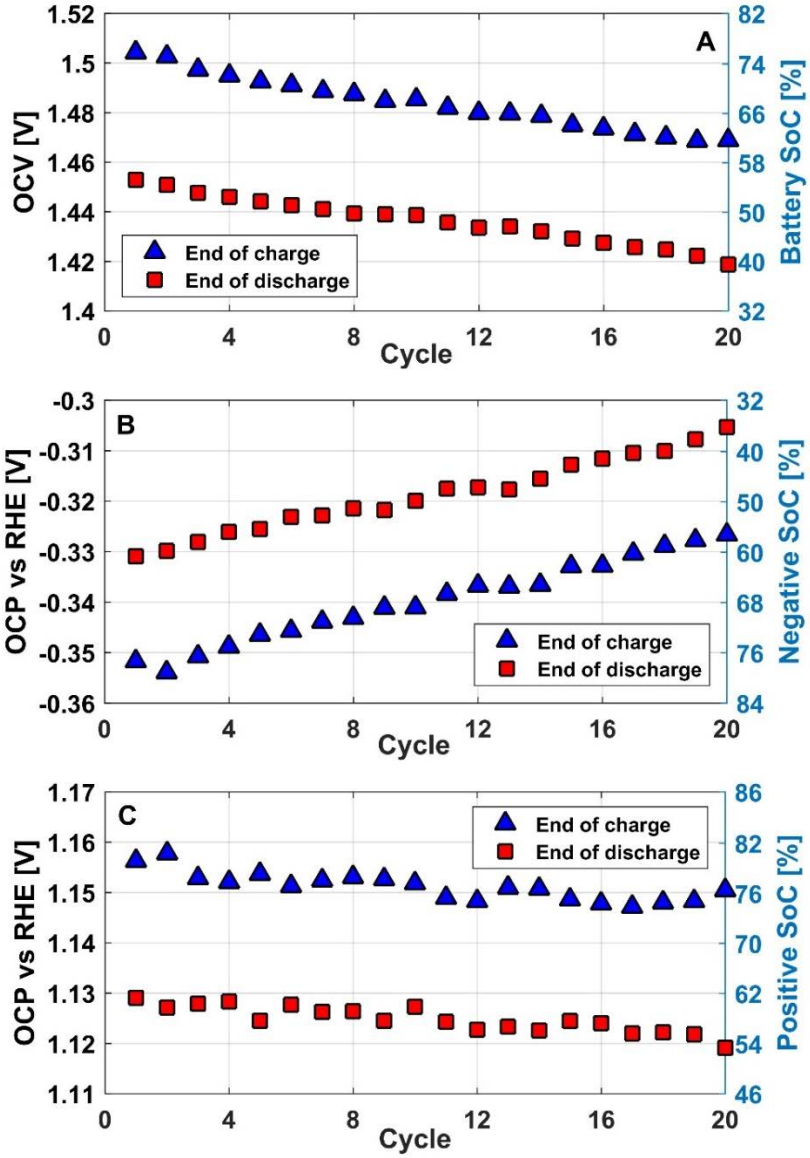

Figure 7 – Evolution during 20 charge-discharge cycles at 50 mA cm^{-2} of A) cell OCV and battery SoC; B) negative electrode OCP and SoC; C) positive electrode OCP and SoC.

During battery operation vanadium ions transport through the membrane is regulated by a complex interplay between convection, diffusion and migration mechanisms; in order to provide a more solid interpretation of experimental data modeling analysis is necessary, but this is out of the scope of this work.

The presented investigation highlights the importance of having reliable reference electrodes in VRFB, that are able to monitor electrolyte and local electrode potentials during system operation, evidencing which component or which region of the cell is undergoing severe

degradation and providing useful insight into component replacement and development of suitable operating strategies.

4. Conclusions

In this work, through-plate reference electrodes are introduced at inlet and outlet of both positive and negative VRFB electrodes, providing an insight into the evaluation of local overpotentials and electrolytes imbalance during system cycling. The system of through-plate reference hydrogen electrodes consists in salt bridges passing through the end plates of the cell, creating an ionic contact between the electrode and a reference hydrogen electrode placed outside the cell.

The main conclusions of the work are the following:

- The obtained relations between positive and negative electrolyte potential and the corresponding SoC are coherent with Nernst's law. Moreover the difference between the measured cell OCV and the one calculated as the difference between the acquired positive and negative electrode OCP is always included in 5 mV, confirming the reliability of the developed measurement setup.
- The negative electrode presents generally higher overpotentials compared to the positive; the former is kinetically dominated, while the latter exhibits mass transport effects at high current, that are enhanced at cell outlet.
- Local impedance spectra at low current evidence the kinetic limitations of negative electrode, while the positive exhibits a more pronounced impedance feature at low frequency, addressed to mass transport phenomena.
- During cycles at 100 mA cm^{-2} with fixed cut-off voltages the VRFB exhibits strong reduction of capacity and energetic efficiency, that are induced by a coupled effect of electrode degradation and cross-contamination. Reference electrodes measurements

reveal that positive electrolyte is discharged towards higher state of charge, while the negative is charged towards lower state of charge.

- During cycles at 50 mA cm^{-2} with fixed capacity it is possible to clearly highlight the effect of cross-contamination: in the investigated operating conditions it strongly reduces the SoC of the negative electrolyte, while at the positive has got a minor influence.

Acknowledgement

This work was funded by Fondi di Ateneo per la Ricerca di Base of Politecnico di Milano. The authors would like to thank Mirko Messaggi and Dr. Claudio Rabissi for the helpful support in the experimental measurements.

References

[1] P. Alotto, M. Guarnieri, F. Moro, Redox flow batteries for the storage of renewable energy: A review, Renewable and Sustainable Energy Reviews. 29 (2014) 325–335. doi:10.1016/j.rser.2013.08.001.

[2] G.L. Soloveichik, Flow Batteries: Current Status and Trends, Chemical Reviews. 115 (2015) 11533–11558. doi:10.1021/cr500720t.

[3] A. Parasuraman, T.M. Lim, C. Menictas, M. Skyllas-Kazacos, Review of material research and development for vanadium redox flow battery applications, Electrochimica Acta. 101 (2013) 27–40. doi:10.1016/j.electacta.2012.09.067.

[4] A.Z. Weber, M.M. Mench, J.P. Meyers, P.N. Ross, J.T. Gostick, Q. Liu, Redox flow batteries: A review, Journal of Applied Electrochemistry. 41 (2011). doi:10.1007/s10800-011-0348-2.

[5] X.L. Zhou, Y.K. Zeng, X.B. Zhu, L. Wei, T.S. Zhao, A high-performance dual-scale porous

electrode for vanadium redox flow batteries, Journal of Power Sources. 325 (2016) 329–336. doi:10.1016/j.jpowsour.2016.06.048.

[6] M.H. Chakrabarti, N.P. Brandon, S. a. Hajimolana, F. Tariq, V. Yufit, M. a. Hashim, M. a. Hussain, C.T.J. Low, P.V. Aravind, Application of carbon materials in redox flow batteries, Journal of Power Sources. 253 (2014) 150–166. doi:10.1016/j.jpowsour.2013.12.038.

[7] B. Zakeri, S. Syri, Electrical energy storage systems: A comparative life cycle cost analysis, Renewable and Sustainable Energy Reviews. 42 (2015) 569–596. doi:10.1016/j.rser.2014.10.011.

[8] Y.K. Zeng, T.S. Zhao, L. An, X.L. Zhou, L. Wei, A comparative study of all-vanadium and iron-chromium redox flow batteries for large-scale energy storage, Journal of Power Sources. 300 (2015) 438–443. doi:10.1016/j.jpowsour.2015.09.100.

[9] K.W. Knehr, E. Agar, C.R. Dennison, A.R. Kalidindi, E.C. Kumbur, A Transient Vanadium Flow Battery Model Incorporating Vanadium Crossover and Water Transport through the Membrane, Journal of the Electrochemical Society. 159 (2012) A1446–A1459. doi:10.1149/2.017209jes.

[10] S. Corcuera, M. Skyllas-Kazacos, State-of-Charge Monitoring and Electrolyte Rebalancing Methods for the Vanadium Redox Flow Battery, European Chemical Bulletin. 1 (2012) 511–519. doi:10.17628/ECB.2012.1.511.

[11] D. Aaron, C.-N. Sun, M. Bright, A.B. Papandrew, M.M. Mench, T.A. Zawodzinski, In Situ Kinetics Studies in All-Vanadium Redox Flow Batteries, ECS Electrochemistry Letters. 2 (2013) A29–A31. doi:10.1149/2.001303eel.

[12] J. Grosse Austing, C. Nunes Kirchner, E.M. Hammer, L. Komsiyska, G. Wittstock, Study of an unitised bidirectional vanadium/air redox flow battery comprising a two-layered cathode, Journal of Power Sources. 273 (2015) 1163–1170. doi:10.1016/j.jpowsour.2014.09.177.

[13] C. Choi, Y. Choi, S. Kim, H. young Jung, H.T. Kim, Resistor Design for the Use of Dynamic Hydrogen Electrode in Vanadium Redox Flow Batteries, Electrochimica Acta. 213 (2016) 490–495. doi:10.1016/j.electacta.2016.07.152.

[14] H.H. Dewage, V. Yufit, N.P. Brandon, Study of Loss Mechanisms Using Half-Cell Measurements in a Regenerative Hydrogen Vanadium Fuel Cell, Journal of The Electrochemical Society. 163 (2016) A5236–A5243. doi:10.1149/2.0301601jes.

[15] C.-N. Sun, F.M. Delnick, D.S. Aaron, A.B. Papandrew, M.M. Mench, T.A. Zawodzinski, Probing Electrode Losses in All-Vanadium Redox Flow Batteries with Impedance Spectroscopy, ECS Electrochemistry Letters. 2 (2013) A43–A45. doi:10.1149/2.001305eel.

[16] Q. Liu, A. Turhan, T.A. Zawodzinski, M.M. Mench, In situ potential distribution measurement in an all-vanadium flow battery, Chemical Communications. 49 (2013) 6292. doi:10.1039/c3cc42092b.

[17] J. Langner, J. Melke, H. Ehrenberg, C. Roth, Determination of Overpotentials in All Vanadium Redox Flow Batteries, ECS Transactions. 58 (2014) 1–7. doi:10.1149/05837.0001ecst.

[18] I. Derr, a. Fetyan, K. Schutjajew, C. Roth, Electrochemical analysis of the performance loss in all vanadium redox flow batteries using different cut-off voltages, Electrochimica Acta. 224 (2017) 9–16. doi:10.1016/j.electacta.2016.12.043.

[19] G. Hinds, E. Brightman, In situ mapping of electrode potential in a PEM fuel cell, Electrochemistry Communications. 17 (2012) 26–29. doi:10.1016/j.elecom.2012.01.007.

[20] A.M. Pezeshki, R.L. Sacci, F.M. Delnick, D.S. Aaron, M.M. Mench, Elucidating effects of cell architecture, electrode material, and solution composition on overpotentials in redox flow batteries, Electrochimica Acta. 229 (2017) 261–270.

doi:10.1016/j.electacta.2017.01.056.

[21] M. Zago, A. Casalegno, Physically-based impedance modeling of the negative electrode in All-Vanadium Redox Flow Batteries: insight into mass transport issues, Electrochimica Acta. 248 (2017) 505–517. doi:10.1016/j.electacta.2017.07.166.

[22] D.S. Aaron, Q. Liu, Z. Tang, G.M. Grim, A.B. Papandrew, A. Turhan, T.A. Zawodzinski, M.M. Mench, Dramatic performance gains in vanadium redox flow batteries through modified cell architecture, Journal of Power Sources. 206 (2012) 450–453. doi:10.1016/j.jpowsour.2011.12.026.

[23] M. Pavelka, F. Wandschneider, P. Mazur, Thermodynamic derivation of open circuit voltage in vanadium redox flow batteries, Journal of Power Sources. 293 (2015) 400–408. doi:10.1016/j.jpowsour.2015.05.049.

[24] K.W. Knehr, E.C. Kumbur, Open circuit voltage of vanadium redox flow batteries: Discrepancy between models and experiments, Electrochemistry Communications. 13 (2011) 342–345. doi:10.1016/j.elecom.2011.01.020.

[25] A. Tang, J. Bao, M. Skyllas-Kazacos, Dynamic modelling of the effects of ion diffusion and side reactions on the capacity loss for vanadium redox flow battery, Journal of Power Sources. 196 (2011) 10737–10747. doi:10.1016/j.jpowsour.2011.09.003.

[26] D. Aaron, S. Yeom, K.D. Kihm, Y. Ashraf Gandomi, T. Ertugrul, M.M. Mench, Kinetic enhancement via passive deposition of carbon-based nanomaterials in vanadium redox flow batteries, Journal of Power Sources. 366 (2017) 241–248. doi:10.1016/j.jpowsour.2017.08.108.

[27] M.P. Manahan, Q.H. Liu, M.L. Gross, M.M.Mench, Carbon nanoporous layer for reaction location management and performance enhancement in all-vanadium redox flow batteries, Journal of Power Sources. 222 (2013) 498–502. doi:10.1016/j.jpowsour.2012.08.097.

[28] Q. Xu, T.S. Zhao, C. Zhang, Effects of SOC dependent electrolyte viscosity on performance of vanadium redox flow batteries, Applied Energy. 130 (2014) 139–147.

[29] C. Blanc, Modeling of a vanadium redox flow battery electricity storage system, Laboratoire d'Electronique Industrielle. PhD Thesis (2009) 263. doi:10.5075/epfl-thesis-4277.

[30] A. Mousa, M. Skyllas-kazacos, Physical Properties of Negative Half-Cell Electrolytes in the Vanadium Redox Flow Battery, Electrochemically Enabled Sustainability. (2014) 395–428.

[31] J. Xi, S. Xiao, L. Yu, L. Wu, L. Liu, X. Qiu, Broad temperature adaptability of vanadium redox flow battery - Part 2: Cell research, Electrochimica Acta. 191 (2016) 525–534. doi:10.1016/j.electacta.2016.01.165.

[32] X. Li, J. Xiong, A. Tang, Y. Qin, J. Liu, C. Yan, Investigation of the use of electrolyte viscosity for online state-of-charge monitoring design in vanadium redox flow battery, Applied Energy. 211 (2018) 1050–1059. doi:10.1016/j.apenergy.2017.12.009.

[33] M. Messaggi, P. Canzi, R. Mereu, A. Baricci, F. Inzoli, A. Casalegno, M. Zago, Analysis of flow field design on vanadium redox flow battery performance: Development of 3D computational fluid dynamic model and experimental validation, Applied Energy. 228 (2018) 1057–1070. doi:10.1016/ j.apenergy.2018.06.148.

[34] I. Derr, M. Bruns, J. Langner, A. Fetyan, J. Melke, C. Roth, Degradation of all-vanadium redox flow batteries (VRFB) investigated by electrochemical impedance and X-ray photoelectron spectroscopy: Part 2 electrochemical degradation, Journal of Power Sources. 325 (2016) 351–359. doi:10.1016/j.jpowsour.2016.06.040.